https://doi.org/10.5194/acp-2021-266
Preprint. Discussion started: 4 May 2021

Atmospheric Chemistry and Physics Discussions
Open Access
EGU

Measurement Report: New particle formation characteristics at an urban and a mountain station in Northern China

Ying Zhou[1], Simo Hakala[2], Chao Yan[1,2,*], Yang Gao[3], Xiaohong Yao[3], Biwu Chu[4], Tommy Chan[2], Juha Kangasluoma[1,2], Shahzad Gani[2], Jenni Kontkanen[2] , Pauli Paasonen[2] , Yongchun Liu[1], Tuukka Petäjä[2,5], Markku Kulmala[1,2], Lubna Dada[2,*]

[1] Aerosol and Haze Laboratory, Beijing Advanced Innovation Center for Soft Matter Science and Engineering, Beijing University of Chemical Technology, Beijing, China

[2] Institute for Atmospheric and Earth System Research / Physics, Faculty of Science, University of Helsinki, Finland

[3] Key Laboratory of Marine Environment and Ecology, Ministry of Education, Ocean University of China, Qingdao 266100, China

[4] State Key Joint Laboratory of Environment Simulation and Pollution Control, Research Center for Eco-Environmental Sciences, Chinese Academy of Sciences, Beijing 100085, China

[5]Joint International Research Laboratory of Atmospheric and Earth System Sciences (JirLATEST), Nanjing University, Nanjing, China

Correspondence to: Lubna Dada: lubna.dada@helsinki.fi & Chao Yan: chao.yan@helsinki.fi

Abstract

Atmospheric new particle formation (NPF) events have attracted increasing attention for their contribution to the global aerosol number budget, and therefore their effects on climate, air quality, and human health. NPF events are regarded as a regional phenomenon, occurring over a large area. However, the spatial variation of NPF intensity has not been investigated in detail by incorporating both urban and regional measurements. Urban environments have more heterogeneous and freshly emitted NPF precursors as compared to environments with less anthropogenic activity. Here, we provide a comparison of NPF event characteristics — NPF event frequency, particle formation rate, and growth rate — by comparing an urban Beijing site and a background mountain site separated by ~80 km from June 14 to July 14, 2019 as well as give insights into the connection between both locations. During the measurement period, 12 and 13 NPF events were observed at the urban and background mountain sites, respectively, with 9 NPF events observed on the same day at both sites. Although the median condensation sink during the first two hours of the common NPF events was

https://doi.org/10.5194/acp-2021-266
Preprint. Discussion started: 4 May 2021

Atmospheric Chemistry and Physics
Discussions

around 0.01 s^{-1} at both sites, there were notable differences in particle formation rates between the two locations (median of 5.42 $cm^{-3}s^{-1}$ at the urban site and 1.13 $cm^{-3}s^{-1}$ at the mountain site during the first two hours of common NPF events). Yet, the particle growth rates in the 7-15 nm range for common NPF events were comparable (median of 7.6 $nm.h^{-1}$ at the urban site and 6.5 $nm.h^{-1}$ at the mountain site as median values). To understand whether the observed events were connected, we compared air mass trajectories as well as meteorological conditions at both stations. Favorable conditions for the occurrence of regional NPF events were largely affected by air mass transport. Overall, our results demonstrate a clear inhomogeneity of regional NPF within a distance of ~100 km, which should be considered in regional-scale aerosol models when estimating the budget of aerosol load and cloud condensation nuclei.

Keywords: atmospheric aerosols, growth rates, regional new particle formation, haze, sulfuric acid

1 Introduction

Atmospheric new particle formation (NPF) events resulting from the formation of clusters and stable aerosol particles from gas-phase precursors have been recognized as a major contributor to the global aerosol budget (Kulmala et al., 2004;Zhang et al., 2012). Once the newly formed particles grow to certain sizes, they can act as cloud condensation nuclei (CCN), affecting the regional and global climate (Pierce and Adams., 2009;Yu and Luo., 2009). NPF events were also found to contribute to haze formation and thus can influence air quality, especially in megacities where the precursor concentrations and associated particle formation rates are rather high (Guo et al., 2014;Guo et al., 2020;Kulmala et al., 2021, Du & Dada et al. 2021).

The occurrence of NPF events is a result of the competition between factors promoting and inhibiting cluster formation and their growth. For instance, sufficient sulfuric acid and other low-volatility vapors have been confirmed to be important in particle nucleation and growth in field observations as well as in chamber experiments (Ehn et al., 2014;Wang et al., 2017;Lehtipalo et al., 2018;Yao et al., 2018;Deng et al., 2020a). On the other hand, background particles can inhibit new particle formation by acting as condensation sink for vapor precursors and coagulation sink for newly formed particles. Indeed, Cai et al. (2017) found that the Fuchs Surface Area (A_{Fuchs}) (which is linearly proportional to condensation sink) determined the occurrence of NPF events in urban Beijing. In the atmosphere, ambient conditions, such as air mass trajectories and meteorological conditions, can affect the occurrence of NPF events by modifying the source-sink competition. Wu et al. (2007) summarized favorable conditions for NPF events in Beijing based on a one-year observation as sufficient solar radiation (sunny days), northerly wind, low relative humidity, and less pre-loading large particles. Similarly, in other environments, plenty of radiation, intermediate temperatures and low condensation sink favor the occurrence of NPF events (Qi et al., 2015;Dada et al., 2017;Kerminen et al., 2018).

Regional NPF events can happen with a spatial extent up to several hundred kilometers and vertical extent from boundary layer to free troposphere under favorable conditions (Hussein et al., 2009;Shen et al., 2011;Dai et al., 2017). Earlier studies have shown that regional NPF events by simultaneous observations at two or more sites had similar features in their occurrence and characteristics. For instance, Komppula et al. (2006) investigated the occurrence of NPF events at two forest stations in northern Finland during 2000-2003. Their results suggested that same air mass source regions, favorable weather conditions and clean air at both stations were necessary for NPF events occurring simultaneously at the two stations. Vana et al. (2016) compared observations at three sites over 1000 km distance at northern Finland, southern Finland and Estonia in 2013-2014. They found that some events have the same origin. On the other hand, Jun et al. (2014) observed that NPF events occurred less frequently at downtown Toronto than at a nearby background site, and attributed this observation to the high condensation and coagulation sink due to primary particle emission from traffic at urban areas. Moreover, Carnerero et al. (2018) observed horizontal distribution and regional impact of the NPF events with data from three urban, urban background, and suburban stations in the Madrid metropolitan area, Spain in July 2016. Their results indicated that ultra-fine particles were detected quasi-homogenously in an area spanning at least 17 km horizontally and the NPF events extended over the full vertical extension of the mixed layer. Finally, Salma et al. (2016) found that regional NPF events were modified and transformed by urban NPF events during their observation in 2008-2009 and 2012-2013 in Budapest and at a regional background site 71 km away from it.

In comparison to the aforementioned studies in Europe, a similar study was also carried out to understand the regional NPF events in North China Plain. Wang et al. (2013) characterized the NPF events observed at an urban Beijing site and a regional background site about 120 km northeast to the urban site from March to November in 2008. They observed 96 and 87 NPF events at urban Beijing and background site, respectively, among which 52 NPF events were observed simultaneously at both sites. They found that NPF events were slightly weaker in the background site compared to those observed at the urban site. However, the factors that influence the occurrence of NPF events at the two stations simultaneously were left undetermined. In addition to largely populated urban areas, there is a large mountain area within the Beijing-Tianjin-Hebei (BTH) region, where to our best knowledge, the characteristics of NPF events are understudied. In this study, we conducted simultaneous measurements of NPF event characteristics at an urban site in Beijing and a background mountain site about 80 km west to urban Beijing from June 14 to July 14 2019.

Based on our observations, we aim to (i) compare the characteristics of the NPF events between the two sites, including the frequency, particle formation rate, and particle growth rate; (ii) figure out the connections and differences between NPF events at these two sites; (iii) identify the favoring conditions for regional NPF events. Due to the profound participation of NPF events in the global aerosol number loading and air quality degradation, identifying the conditions that promote or inhibit the occurrence of regional scale NPF events could help minimize its adverse effects.

2 Experiment and methodology

2.1 Sites' description

Urban site: The Beijing University of Chemical Technology - BUCT (39.94° N, 116.31° E) station is located on the fifth floor of a university building inside the west campus of BUCT. The station is surrounded by several main roads with heavy traffic and residential areas and thus, can be considered a typical urban station. More details of this station can be found in Zhou et al. (2020). Observations at the urban site are continuous since January 17, 2018 and were only interrupted for necessary instrument maintenance. The location is referred to as '**UB**' from here after and is shown on the map in Fig. 1.

Mountain site: The Beijing Forest Ecosystem Research Station (39.96° N, 115.43° E) is located in the west of Beijing, referred to as '**MT**' from here after, which is part of the Chinese Ecological Research Network (CERN). It is located in the mountain areas west of Beijing, about 80 km from the urban site; see also in Fig. 1. The altitude of the station is 1170 m above sea level and it is surrounded by forests. The closest anthropogenic activities are associated with small villages located in the valley nearby the MT station. Observations at MT station are from June 14 to July 14, 2019. For comparison reasons, we only used the data collected simultaneously at both stations.

2.2 Instrumentation

Particle number size distribution data in the size range of 6-840 nm were collected using a differential mobility particle sizer (DMPS) at the UB station. The instrument consists of one DMA (differential mobility analyzer) in different flow rates and one CPC (condensation particle counter, TSI Model 3772). Details of this instrument can be found in Kangasluoma et al. (2020). At MT station, a scanning

https://doi.org/10.5194/acp-2021-266
Preprint. Discussion started: 4 May 2021

mobility particle sizer (SMPS) and a fast mobility particle sizer (FMPS, TSI Model 3091) were used to measure particle number size distribution from June 14 to June 28 and from June 29 to July 14, respectively. The size ranges of the SMPS and FMPS are 7-1218 nm and 6.04-856 nm, respectively. The total number concentration from 4-3000 nm, measured by Condensation Particle Counter (CPC; TSI Model 3775), was used to calibrate the particle number size distributions from FMPS according to the method suggested by Zimmerman et al. (2015). More details about the instrument are found in the previous studies (Wang et al., 2019;Gao et al., 2020). The full campaign particle number size distributions at both sites are shown in Fig. 2.

Sulfur dioxide (SO_2) concentration data were collected by Thermo Environmental Instrument model 43i-TLE with a time resolution of 5-min at the UB station. There were no direct measurement of SO_2 concentrations at the MT station, but the SO_2 measurement at the closest national monitoring station (Longquan station, around 60 km from MT station and 20 km from UB station, see Fig. 1) was used to indicate the strong decline of SO_2 concentration from urban Beijing towards the west areas. Time series of SO_2 concentration at UB station and Longquan station during the whole observation is shown in Fig. 3. Due to the lower emission, the SO_2 concentration at the MT station is expected to be even lower than that in Longquan station.

The sulfuric acid concentration was measured at UB station by a chemical ionization-atmospheric interface-time of flight mass spectrometers (CI-APi-ToF, Aerodyne Research Inc.) equipped with a nitrate chemical ionization at UB station (Lu et al., 2019). There were no sulfuric acid data available at MT station and since no SO_2 concentrations were available, a sulfuric acid proxy concentration could not be derived.

The meteorological conditions such as relative humidity (RH, %), temperature (℃) and solar radiation (UVA and UVB, W/m^2) were measured using a Vaisala Weather station data acquisition system (AWS310, PWD22, CL51), Metcon at UB station and using Vaisala MAWS301 automatic weather station at MT station. The measurements at the MT station were carried out at the height of 1.5 m.

https://doi.org/10.5194/acp-2021-266
Preprint. Discussion started: 4 May 2021

2.3 *Air mass back trajectories*

Air mass back trajectories were calculated using a Lagrangian particle dispersion model FLEXPART (FLEXible PARTicle dispersion model) version 9.02 (Stohl et al., 2005). As the meteorological input, we used ECMWF (European Centre for Medium-Range Weather Forecast) operational forecast data with 0.15° horizontal and 1-hour temporal resolution. Particle retroplume simulations were performed hourly for both sites during the whole study period. For each retroplume simulation, we used 50 000 model particles distributed evenly between 0–100 m above the measurement site. The released model particles were traced backwards in time for 72 h, unless they exceeded the model grid (20–60°N, 95–135°E, resolution: 0.05°).

Based on the arrival direction of the 72-h backward trajectories, the prevailing air mass transport conditions at each site were classified into 5 groups: North group, West group, East group, South group and Local group. Air masses arriving from north, north-west and north-east including Mongolia, Inner-Mongolia and north-east China were classified into the North group. Air masses from Shanxi province, Inner-Mongolia and further west were classified into the West group. Air masses from the ocean east of Beijing were classified into the East group and air masses from southern areas were classified into the South group. Stagnant air masses that had only travelled short distances and/or were circulating around the measurement site were classified into the Local group. Examples of air mass trajectories belonging to these five groups are shown in Fig. 4. In general, air masses from the north and west supply clean air from the mountainous areas to both stations, whereas air masses from the east and south travel over highly populated areas, thus accumulating air pollutants. However, the impact of local air masses on the pollution levels at the two sites can be different; at UB station, local air masses are polluted by the urban emissions, while at MT station stagnant air could cause a clean situation due to low local emissions. More details on the relationship between air mass transport conditions and the extent of pollution is discussed in later sections.

2.4 *NPF event classification*

Particle number size distribution data from both stations were used for classifying individual days

https://doi.org/10.5194/acp-2021-266
Preprint. Discussion started: 4 May 2021

Atmospheric Chemistry and Physics Discussions

into new particle formation (NPF) event days and non-event days. This classification followed procedures presented by Dal Maso et al. (2005) and later adapted for urban locations (Chu et al., 2021) in which a day is classified as a NPF event day if (a) a new mode in the size range smaller than 25 nm appeared and (b) the new mode kept growing over several hours. On the other hand, non-event days are the days which do not fit any of the abovementioned criteria and undefined days are the days which fit either one of the abovementioned criteria or the days which we cannot distinguish whether the new mode was from NPF event or traffic.

2.5 Characteristics of NPF events

2.5.1 Condensation sink

The condensation sink (CS) was calculated from particle size distribution data using the method described by Kulmala et al. (2012):

$$CS = 2\pi D \sum_{dp'} \beta_{m,dp'} dp' N_{dp'} \quad (1)$$

where D is the diffusion coefficient of the condensing vapor, sulfuric acid in our case, and $\beta_{m,dp'}$ represents the transition-regime correction, $N_{dp'}$ is the particle number concentration with diameter dp'. As shown in Fig. 5, particles in size range of 20-800 nm dominated the total CS at UB station and particles in the size range of 50-800 nm dominated the total CS at MT station. Although the size ranges of DMPS, FMPS and SMPS slightly differ, all of them cover the main size range which constituted the CS and thus the calculation of CS should not be significantly influenced by differences in the instrument size ranges.

2.5.2 Particle growth rates

Particle growth rates were calculated for the size range of 7-15 nm ($GR_{7\text{-}15\ nm}$) using the 50% appearance time method introduced by Lehtipalo et al. (2014) and Dada et al. (2020b) according to

$$GR = \frac{dp_2 - dp_1}{t_2 - t_1} \quad (2)$$

where t_2 and t_1 are the appearance times of particles with sizes of dp_2 and dp_1, respectively. The

https://doi.org/10.5194/acp-2021-266
Preprint. Discussion started: 4 May 2021

appearance time is defined as the time at which the concentration of particles at size d_p reaches 50% of its maximum.

2.5.3 *Particle formation rates*

The formation rates of particles of diameters 7 nm (J_7) were calculated from particle number size distribution data using the method presented by Kulmala et al. (2012) and modified for urban environments by Cai and Jiang (2017):

$$J_k = \frac{dN_{[d_k,d_u)}}{dt} + \sum_{d_g=d_k}^{d_{u-1}} \sum_{d_i=d_{\min}}^{+\infty} \beta_{(i,g)} N_{[d_i,d_{i+1})} - \frac{1}{2} \sum_{d_g=d_{\min}}^{d_{u-1}} \sum_{d_i^3=\max(d_{\min}^3, d_k^3-d_{\min}^3)}^{d_{i+1}^3+d_{g+1}^3 \le d_u^3} \beta_{(i,g)} N_{[d_i,d_{i+1})} N_{[d_g,d_{g+1})} + \left.\frac{dN}{dd_i}\right|_{d_i=d_u} \bullet GR_u \quad (3)$$

Here, J_k is the particle formation rate at size d_k, $cm^3 \cdot s^{-1}$, (7 nm in this study); d_u is the upper size limit of the targeted aerosol population (10 nm in this study); d_{min} is the smallest particle size detected by particle size spectrometers (to make the results comparable, the d_{min} was set to 7 nm); $N_{[dk,du)}$ is the number concentration of particles from size d_k to d_u; d_i represents the lower limit of the i^{th} size bin; $\beta_{(i,g)}$ is the coagulation coefficient for the collision of two particles with the size of d_i and d_g; and GR_u refers to the particle growth rate at size d_u, $nm \cdot h^{-1}$ (Deng et al., 2020a).

3 Results and discussion

3.1 NPF event characteristics at both stations

3.1.1 NPF event frequency at both stations

In Fig. 2, we show the particle number size distribution and CS during our observations at both stations. There were a total of 12 and 13 NPF events observed at the UB station and the MT station, corresponding to an NPF event frequency of 48% (12 of 25) and 52% (13 of 25), respectively. Only days when there was good data for both stations were taken into consideration in our whole analysis. The NPF event frequencies were higher than earlier long-term observations in urban Beijing and at a background site in Beijing, as well as another observation in 2018 at UB station in which NPF events occurred on less than 20% of the days in summer (Wang et al., 2013;Deng et al., 2020a). One possible reason could be that earlier observations covered the whole summer while our observation only lasted for 31 days (where 25 days were validated data), and some parameters affecting NPF event occurrence could vary from month to month as well as from year to year. In addition, 9 NPF events were observed at both stations on the same day (referred to as common NPF events). Detailed information on the classified NPF event and non-event days, including the particle formation rates, growth rates, as well as their associated air mass origins are provided in Table 1.

3.1.2 NPF event start time at both stations

During our observation, there was no advection of air masses between the two sites on common NPF event days, indicating that the NPF events occurred at each site independently. As shown in Table 1, all common NPF events started after sunrise and prior to noon except the two non-local NPF events at MT station. However, NPF event start time was different between the two sites. Earlier researches in Nanjing, China and Nordic stations showed the similar results that NPF events can be observed simultaneously at two or more sites, but the start time can be different, local meteorology, source strength and background aerosols could drive temporal behavior of NPF events at each sites (Hussein et al., 2009; Dai et al., 2017).

3.1.3 Particle formation and growth rates at both stations

The particle formation rates (J_7) at the two stations during the measurements are shown in Fig.6a. The J_7 at the UB station (3.0-10.0 $cm^{-3}\,s^{-1}$ with a median of 5.4 $cm^{-3}\,s^{-1}$) was significantly higher than that in the MT station (0.75-3.0 $cm^{-3}\,s^{-1}$ with a median of 0.72 $cm^{-3}s^{-1}$) for common NPF events. These values are comparable to earlier observations in urban Beijing and another regional background station in North China Plain (NCP) (Wang et al., 2013). Earlier observations in NCP and Yangtze River Plain also observed higher formation rates at urban sites than corresponding background sites by roughly a factor of 2 due to lower anthropogenic emissions at background sites (Wang et al., 2013;Dai et al., 2017;Shen et al., 2018). The much lower J_7 observed at MT station is very likely associated with the low H_2SO_4 concentration at this station, which we will discuss in section 3.2.4. However, other reasons, such as the low concentration of H_2SO_4 stabilizers, e.g., amines, cannot be

https://doi.org/10.5194/acp-2021-266
Preprint. Discussion started: 4 May 2021

ruled out either. Also, the J_7 at UB station could be affected by particle emissions due to the proximity of the location to the highway (Kontkanen et al., 2020).

In contrast to the significant difference of J_7, the median particle growth rates in size range of 7-15 nm ($GR_{7\text{-}15nm}$) were similar between the two stations, with 7.6 nm/h and 6.5 nm/h at the UB station and the MT station, respectively (Fig. 6b). The GR at UB station was comparable with other long-term observation at UB station (1.1-8.0 nm/h) in 2018, and other urban areas in China (Herrmann et al., 2014;Chu et al., 2019;Deng et al., 2020a). Consistent with earlier observations showing that H_2SO_4 could only contribute to a small fraction of the particle growth at this size range (Paasonen et al., 2018;Qi et al., 2018;Guo et al., 2020), the growth rates at both stations cannot be explained by the H_2SO_4 concentration. This implies that other condensable species, very likely low-volatility organic vapors, play an important role in particle growth at both stations. At the UB station, anthropogenic VOCs are dominant precursors of these low-volatility organic vapors (Guo et al., 2020; Deng et al., 2020b), while VOCs at MT station, with rare anthropogenic sources, are likely dominated by biogenic emissions.

3.1.4 Ending diameters of newly- formed grown particles

Earlier observations found that diameters of newly-formed particles should be larger than 70 nm to contribute to cloud condensation nuclei significantly (Man et al., 2015; Ma et al., 2021) and will be considered as haze particles when their size larger than 100 nm (Kulmala et al. 2021). However as shown in Table 1, the maximum mode diameters of the newly grown particles (D_{pmax}) varies from 21 to 105 nm at the UB station and 19 to 102 nm at MT station and D_{pmax} of common NPF events were higher at UB than MT station. At UB station there were 4 NPF events with D_{pmax} larger than 70 nm, while only one such event was observed at MT station. The higher ending diameters of the newly-formed grown particles indicates more abundant vapors favoring the growth of larger particles at UB than MT station. The result also suggests that NPF events at urban areas may have larger impacts on haze and climate than those at clean areas.

https://doi.org/10.5194/acp-2021-266
Preprint. Discussion started: 4 May 2021

3.2 Factors influencing the occurrence of NPF events

In order to understand the conditions favoring NPF events at both stations, we analyzed various ambient parameters including air mass trajectories, meteorological variables, condensation sink as well as sulfuric acid concentration.

3.2.1 Favorable air mass origin for NPF events at individual locations

Due to the close proximity of the two measurement sites, the air mass arrival directions and source regions were (mostly) similar at both sites throughout the measurement period. Frequencies of air masses arriving at each station from every group are shown in Fig. 7. The most frequent air masses arriving at both sites belonged to the North and East groups. At the UB site, out of 25 days there were 8 days belonging to each of the North and East groups and 1, 1 and 7 days in air masses belonging to West, South and Local groups, respectively. For the MT station, there were out of 25 days, 9 and 6 belonged to the North and East groups, respectively, and 3 and 7 days belonged to West, Local groups, respectively.

NPF event frequency with respect to air masses is shown in Fig. 7. It is noticeable that air mass origin influenced the occurrence of NPF events at both stations– as the highest frequency of NPF events occurred when the air masses were coming from the north. The second highest frequency of NPF events was observed when the air mass belonged to the Local group (Fig. 7a&b). At UB station, 11 (out of 12) NPF events occurred in these two air mass classes (North and South groups), with another NPF event in the West group. For the MT station, 11 (out of 13) NPF events occurred in these two air mass classes (North and South groups), with two other NPF events in the West and East groups. Considering the comparable NPF frequency associated with the North and South group, the difference in the CS remains one prominent difference between them. As shown in Fig. 7c&d, the CS of the air masses classified as the North group (with median values of 0.01 s^{-1} at both stations) is substantially lower than that in other air mass classes, which might be a main reason for the high NPF event frequency associated with this air mass class. This result is consistent with earlier researches that air masses from north favored NPF occurrence by low CS in North China Plain (Wang et al., 2013;Shen et al., 2018). On the other hand, despite the highest CS of the air masses in Local group (with median

https://doi.org/10.5194/acp-2021-266
Preprint. Discussion started: 4 May 2021

Atmospheric Chemistry and Physics Discussions

values of 0.025 and 0.028 s^{-1} at the UB station and MT station, respectively, on NPF event days), NPF event could still occur in this air mass class. This is likely due to the high concentrations of cluster forming vapors that act as particle sources outcompeting the high CS in these cases.

As shown in Table 1, NPF events occurring simultaneously at both sites only happened when air masses arrived at both sites from the same directions, suggesting that most of the observed NPF events took place over the whole studied area, extending for several hundreds of kilometers (Dai et al., 2017, Du et al. 2021). The occurrences of common NPF events also closely connected with air mass origins that 7 (out of 9) common NPF events occurred under air masses in the North group, with the other two NPF events in the South group.

3.2.2 The role of the condensation sink in NPF event occurrence

Figure 8 shows the difference in CS on NPF event and non-event days at the two stations. On NPF event days, the median CS was ~ 0.01 s^{-1} during the first 2 hours of the NPF events, at both stations. On common NPF event days, the median CS was 0.009 s^{-1} at UB station and ~0.01s^{-1} at MT station, respectively. In comparison, on non-event days, during roughly the same time period (9:00–11:00 LT), the CS was substantially higher, with median values of 0.02 s^{-1} and 0.014 s^{-1}, at UB and MT stations, respectively. The median CS on NPF event days during our measurement period was lower than those previously reported values based on long-term data which was 0.027 s^{-1} and 0.019 s^{-1} at two sites in urban Beijing respectively (Wang et al., 2013;Deng et al., 2020a). This could be attributed to a shorter studied period in our study as well as changes in meteorological conditions in comparison to previous years.

As shown in Fig. 9a&b, when CS was smaller than 0.015 s^{-1}, most (10 out of 11) days were classified as NPF event days. When CS was larger than 0.032 s^{-1}, all days were classified as non-event days. When CS was between 0.015 and 0.032 s^{-1}, there were only 2 NPF event days, 4 undefined days and 4 non-event days. Different from NPF events under low CS (<0.015 s^{-1}), these two NPF events under high CS were characterized by a relatively high H_2SO_4 concentration (>10^7 cm^{-3}) and low particle formation rates, discussed in further details in the coming sections. This result is consistent with long-term observations at UB station during 2018 (Jan 16–May 17 and Oct19–Dec 26) and 2019 (Jan 1–

https://doi.org/10.5194/acp-2021-266
Preprint. Discussion started: 4 May 2021

Mar 28 and Jul 19–Dec 31) (Deng et al., 2020a). As well as at another site in urban Beijing during 2016 (Mar 7–Apr 6) during which NPF event days dominated the measured days when CS was smaller than 0.01 s^{-1}, and NPF events rarely happened when CS was larger than ~ 0.03 s^{-1} (Deng et al., 2020a). In comparison, at MT station, when CS was smaller than ~ 0.013 s^{-1}, most (10 out of 14) days were classified as NPF event days as shown in Fig. 9d. When CS was larger than ~0.013 s^{-1}, we only observed one local NPF event and another two non-local NPF events (the non-local NPF events will be discussed in section 3.3.2). The local NPF event under high CS at the MT station was characterized as high UV (>30 W/m^2) and low formation rate (J_7 were too small to be reliably calculated) as well.

3.2.3 Role of meteorological variables in NPF event occurrence

While the air mass source regions, and their connection to the CS, seem to explain the general picture of NPF event occurrences at the two sites well, we still have some cases unexplained. For example, as shown in Table 1, there were several non-event days observed at MT station with air masses belonging to North and West groups, which were connected to low CS. This indicates that a further investigation into other NPF-related variables is still required.

First, the intensity of solar radiation is considered one of the most important parameters deciding NPF event occurrence as it translates into photochemistry strength (Chu et al., 2019). The median UV (UVA+UVB) intensity at the UB station on NPF event and non-event days was 38.3 and 32.9 W/m^2, respectively. The UV intensity was on average ~15% higher on NPF event days than on non-event days at UB station. Although UV intensity was important for NPF event occurrence, we still observed NPF events at UB station under low UV intensity, e.g. cases on June 30 and July 6 as shown in Fig. 9a. These two events all started immediately after sunrise (6:30 LT on June 30 and 7:00 LT on July 6, see Table 1) and median UV intensity during the first two hours of NPF events was only 13.2 and 14.1 W/m^2 (Fig. 9b), respectively. However, sulfuric acid concentration was higher than 10^7 cm^{-3} at the same time, the possible reason is high SO_2 concentration and low CS (~0.003 s^{-1}, see Fig. 9a) outcompeted the low UV intensity (Dada et al., 2020a) as well as the possibility of having other H_2SO_4 sources (Yao et al., 2020).

https://doi.org/10.5194/acp-2021-266
Preprint. Discussion started: 4 May 2021

At MT station, the median UV intensity on NPF event and non-event days was 28.4 and 14.2 W/m^2, respectively. The lower UV at MT station, in general might be related to the higher RH (Fig. 10c&d) and thus more cloudiness and fog at the MT station (Hamed et al., 2010;Dada et al., 2018). The UV intensity was on average ~100% higher on NPF event days than on non-event days at UB station. All local NPF events happened when UV intensity was higher than 15 W/m^2 as shown in Fig. 9c.

On the other hand, as shown in Fig. 10c&d, the median relative humidity (RH) was lower on NPF event days than non-event days at both stations. This is consistent with earlier results that high RH suppressed NPF events by increasing CS and coagulation sink (CoagS), as it can enhance the particle hygroscopic growth (Hamed et al., 2010;Hamed et al., 2011). In addition, high RH was also found to be associated with more clouds resulting in less solar radiation (Dada et al., 2018).

The median temperatures at UB on event and non-event days were 31 °C and 29 °C, respectively, and at MT station 23 °C and 19 °C, respectively. The median temperature was lower at the MT station than at the UB station, due to the higher altitude of the station and likely also the weaker solar radiation (Fig. 10a&b). At both stations, the median temperature was very similar on NPF events and non-event days, suggesting that temperature was not a crucial factor for NPF event occurrence during the measurement.

3.2.4 Role of Sulfuric acid concentrations in NPF event occurrence

Besides having favorable conditions such as low CS and sufficient radiation, the occurrence of NPF event requires a sufficient concentration of precursor vapors. Sulfuric acid has been found to be the main precursor vapour participating in NPF in China and in many locations around the world due to its low volatility (Chu et al., 2019; Yao et al., 2018). In Fig. 9a&b, we show the concentration of sulphuric acid as a function of CS. As shown in Fig. 9c, the median sulfuric acid (H_2SO_4) concentrations at UB station were 8.1×10^6 cm^{-3} and 4.5 ×10^6 cm^{-3} on NPF event days and non-event days, respectively. This suggests that H_2SO_4 was important for NPF events at the UB station (Deng et al., 2020a;Dada et al., 2020a). On the other hand, as shown in Fig. 9c, the H_2SO_4 concentration during 9:00- 11:00 (local time) on non-event days could be comparable with that on NPF event days, especially when CS was high. Altogether, our observation shows that the occurrence of NPF events was controlled by both H_2SO_4 and CS at the UB station (Cai et al., 2020).

In addition, although we did not perform the measurement of H_2SO_4 at the MT station, the concentration of H_2SO_4 is expected to be much lower than that at the UB station. First, the SO_2 concentration at measurement at Longquan Town was always below the detection limit (~ 0.5 ppb) during our observation period. In comparison, median SO_2 concentration at UB station was 0.87 ppb for all days and 0.65 ppb for NPF event days during our observation period. The spatial decreasing trend of SO_2 concentration from urban Beijing to the west implies a low SO_2 concentration at the MT station, especially when the nearby anthropogenic sources are sparse (Liu et al., 2008;Yang-Chun et al., 2013;Wang et al., 2011;Ying et al., 2010). Second, the oxidation of SO_2 by photochemistry reactions could also be limited by the low solar radiation at the MT station as we discussed above. Third, CS, as the main sink of H_2SO_4, was comparable at the MT station to that in the UB station. Altogether, the lower production rate and the equivalent loss rate of H_2SO_4 at the MT station likely results in the lower H_2SO_4 concentration, in comparison to UB station.

Due to the lack of H_2SO_4 measurement, the NPF mechanism at the MT station cannot be inferred. Nevertheless, we show that the occurrence of NPF as a response to photochemistry (and very likely to H_2SO_4) and CS in Fig. 9d. It is clear that high UV intensity and low CS favored the occurrence of NPF. However, there existed exceptions. For example, it was an undefined day on June 28 despite of the high UV intensity and low CS. Besides, two NPF events were observed even when the UV intensity was low and the CS was high. These exceptional cases will be discussed in detail in Section 3.3.2.

3.3 Case studies

3.3.1 Non-local NPF events at the MT station

As we discussed above, NPF events at MT stations were favored by strong photochemistry (sufficient solar radiation) and low CS. However, we also observed two NPF events under low solar radiation and high CS on June 15 and 25. These two NPF events had similar characteristics, and we explain the case on June 15 in detail. During this case, air masses arrived at both stations from south-east around 9:00 LT as shown in Fig. 10b&d, resulting in high CS especially at MT station (Fig. 10a&c).

https://doi.org/10.5194/acp-2021-266
Preprint. Discussion started: 4 May 2021

Atmospheric Chemistry and Physics
Discussions
Open Access

The NPF event at the UB station was observed around 11:00 LT, with a high median J_7 of 5.56 $cm^{-3}s^{-1}$, whereas no indication of NPF event at MT was observed until 15:00 likely due to the high CS. After 15:00 LT, a new growing mode from 15 nm appeared at MT station. Because there was no intense increase of sub-15 nm particle number concentration throughout the whole event, the NPF event at MT station was not local but occurred somewhere else and transported to MT station. This a common phenomenon, particularly when the conditions do not favor NPF events to occur on site, but are NPF-favorable somewhere else. The particles formed off-site are transported vertically or horizontally and observed on site (Dada et al., 2018;Leino et al., 2019). Different from other NPF events, this non-local NPF event was associated with strong southerly wind (Fig. 11e), the NPF event observed at the MT station might originate from urban areas 60 km south to the station as shown in Fig.1, assuming the NPF event started around 9:00 and the mean wind speed was 3 m/s.

3.3.2 Undefined day under low CS and high UV condition at MT station

Interestingly, we also observed an undefined day at MT station with low CS (0.006 s^{-1}) and high UV (28 W/m^2) on June 28 (Fig. 9c & Fig. 12c) as there seems to be a very weak 'banana' around 13:00 in the particle number size distribution plot. All other days with such conditions were classified as NPF event days. In this case, the reasonable explanation would be low precursor vapours which we think are SO_2 in our case. On this day, an air mass from Inner-Mongolia arrived at both stations, resulting in very low SO_2 concentration at the UB station among all NPF event days during our observation as shown in Fig. 3. It is reasonable to assume that the SO_2 concentration was even lower at the MT station than at the UB station, and low H_2SO_4 concentration could also be expected, which could be insufficient to trigger an NPF event. This is consistent with an earlier long-term observation at Shangdianzi, another background site of Beijing, where the NPF events were suppressed by air masses from Inner-Mongolia due to the low precursor concentrations (Shen et al., 2018). In comparison, we observed a very weak NPF event at UB station at the same day, as local emissions were enough to supply enough vapors to initiate NPF event.

4 Conclusion

We conducted observations of NPF events at an urban site (UB) and a background mountain site (MT) in Beijing and fully analyzed the favorable conditions for NPF event occurrences at each of the sites. In order to identify the similarities and differences between NPF events at both stations in terms of frequency, intensity and mechanisms, we compared certain NPF characteristics including particle formation rate, growth rate as well as NPF event start time and ending diameters of newly-formed growing particles at both stations. We found that NPF events are most of the time a regional phenomenon occurring over the studied areas and connected closely with air masses source regions during our observation. The air masses from north favored common NPF events more than any other mass trajectories due to their associated clean air masses and thus low CS. Additionally, air masses from the north group always resulted in an NPF event at UB station, while other factors still suppressed their occurrence at the MT station. For example, we found that sufficiently high solar radiation, e.g. UV (UVA+UVB) intensity larger than 15 W/m^2 is required for an NPF event to occur at MT and NPF events observed under solar radiation conditions smaller than 15 W/m^2 were rather transported NPF events from areas upwind to MT station. Another factor suppressing the occurrence of NPF events at MT is the too low precursor gas concentrations (e.g. SO_2) which was visible in MT rather than at UB. Moreover, we found that the CS limit for NPF event occurrence at UB station was ~0.032 s^{-1}, which is consistent with earlier observations in urban Beijing. In comparison, at MT station the CS limit could be only ~0.013 s^{-1}, above which local-NPF events could possibly be suppressed associated with the lower SO_2 concentration.

Although NPF events could happen simultaneously at both stations, the NPF event strength (particle formation rates) was significantly higher at UB than MT station, possibly due to spatial inhomogeneity in the sources of aerosol precursor compounds as well as solar radiation. In comparison, the particle growth rates in size range of 7-15 nm were comparable between these two sites. This clearly suggested that particle formation and further growth are mediated by different vapors. The ending diameters of newly-formed grown particles were higher at UB than MT station, most likely due to the more abundant precursors at the urban area. Our results suggest that NPF events at urban areas could have a bigger influence on global/regional climate and air pollution than those

https://doi.org/10.5194/acp-2021-266
Preprint. Discussion started: 4 May 2021

at clean areas.

NPF events in urban areas were likely transported to regional background sites during our observation. Yet, it remains unknown whether NPF event at regional background sites can affect NPF event in urban areas despite the fact that NPF event and particle growth which are driven by regional air masses can also interact with urban climate (Salma et al., 2016, Du et al. 2021). To fill the knowledge gap, long-term observations on NPF events upwind and downwind urban Beijing are important. Such observations can shed light into the regionality of NPF events and the dynamical development of the aerosol population influenced by radical chemistry in the plume of a megacity. The importance of NPF events as a potential crucial contributor to haze and air pollution in general (Kulmala 2015, Kulmala et al., 2021) need be investigated in not only long-term but also more sites with comprehensive observations (Kulmala, 2018) for better implementations in global models and policy making strategies.

Conflict of interest: The authors declare no competing interests.

Author contributions: YZ, CY, YG, XY performed the measurements. YZ, SH, CY, YG, LD, XY analyzed the data. YZ, CY, SH, LD wrote the manuscript. All authors reviewed the paper and contributed to the scientific discussions.

Data availability: The data displayed in this manuscript will be available online at zenodo.com once the manuscript is in its final publication format.

Financial support: This publication has been produced within the framework of the EMME-CARE project, which has received funding from the European Union's Horizon 2020 Research and Innovation Programme (under grant agreement no. 856612) and the Government of Cyprus. This research has also received funding from the European Commission grant agreement no. 742206 ("ERC-ATM-GTP") as well as Academy of Finland Projects 316114 & 311932. Simo Hakala acknowledges the doctoral programme in Atmospheric Sciences (ATM-DP, University of Helsinki) for financial support. The sole responsibility of this publication lies with the author. The European Union is not responsible for any use that may be made of the information contained therein.

5 References

Cai, R., Yan, C., Yang, D., Yin, R., Lu, Y., Deng, C., Fu, Y., Ruan, J., Li, X., Kontkanen, J., Zhang, Q., Kangasluoma, J., Ma, Y., Hao, J., Worsnop, D. R., Bianchi, F., Paasonen, P., Kerminen, V.-M., Liu, Y., Wang, L., Zheng, J., Kulmala, M., and Jiang, J.: Sulfuric acid-amine nucleation in urban Beijing, Atmos. Chem. Phys. Discuss. [preprint], https://doi.org/10.5194/acp-2020-1060, in review, 2020.

Cai, R., and Jiang, J.: A new balance formula to estimate new particle formation rate: reevaluating the effect of coagulation scavenging, Atmos Chem Phys, 17, 12659-12675, 10.5194/acp-17-12659-2017, 2017.

Cai, R., Yang, D., Fu, Y., Wang, X., Li, X., Ma, Y., Hao, J., Zheng, J., and Jiang, J.: Aerosol surface area concentration: a governing factor in new particle formation in Beijing, Atmos Chem Phys, 17, 12327-12340, 10.5194/acp-17-12327-2017, 2017.

Carnerero, C., Pérez, N., Reche, C., Ealo, M., Titos, G., Lee, H.-K., Eun, H.-R., Park, Y.-H., Dada, L., Paasonen, P., Kerminen, V.-M., Mantilla, E., Escudero, M., Gómez-Moreno, F. J., Alonso-Blanco, E., Coz, E., Saiz-Lopez, A., Temime-Roussel, B., Marchand, N., Beddows, D. C. S., Harrison, R. M., Petäjä, T., Kulmala, M., Ahn, K.-H., Alastuey, A., and Querol, X.: Vertical and horizontal distribution of regional new particle formation events in Madrid, Atmos Chem Phys, 18, 16601-16618, 10.5194/acp-18-16601-2018, 2018.

Chu, B., Dada, L., Liu, Y., Yao, L., Wang, Y., Du, W., Cai, J., Daellenbach, K., Chen, X., Simonen, P., Zhou, Y., Deng, C., Fu, Y., Yin, R., Li, H., He, X.-C., Feng, Z., Yan, C., Kangasluoma, J., and Kulmala, M.: Particle growth with photochemical age from new particle formation to haze in the winter of Beijing, China, Science of The Total Environment., 753, 10.1016/j.scitotenv.2020.142207, 2021.

Chu, B. W., Kerminen, V. M., Bianchi, F., Yan, C., Petäjä, T., and Kulmala, M.: Atmospheric new particle formation in China, Atmos Chem Phys, 19, 115-138, https://doi.org/10.5194/acp-19-115-2019, 2019.

Dada, L., Paasonen, P., Nieminen, T., Mazon, S. B., Kontkanen, J., Peräkylä, O., Lehtipalo, K., Hussein, T., Petäjä, T., Kerminen, V. M., Bäck, J., and Kulmala, M.: Long-term analysis of clear-sky

https://doi.org/10.5194/acp-2021-266
Preprint. Discussion started: 4 May 2021

new particle formation events and nonevents in Hyytiälä, Atmos Chem Phys, 17, 6227-6241, https://doi.org/10.5194/acp-17-6227-2017, 2017.

Dada, L., Chellapermal, R., Buenrostro Mazon, S., Paasonen, P., Lampilahti, J., Manninen, H. E., Junninen, H., Petäjä, T., Kerminen, V.-M., and Kulmala, M.: Refined classification and characterization of atmospheric new-particle formation events using air ions, Atmos Chem Phys, 18, 17883-17893, 10.5194/acp-18-17883-2018, 2018.

Dada, L., Ylivinkka, I., Baalbaki, R., Li, C., Guo, Y., Yan, C., Yao, L., Sarnela, N., Jokinen, T., Daellenbach, K. R., Yin, R., Deng, C., Chu, B., Nieminen, T., Kontkanen, J., Stolzenburg, D., Sipilä, M., Hussein, T., Paasonen, P., Bianchi, F., Salma, I., Weidinger, T., Pikridas, M., Sciare, J., Jiang, J., Liu, Y., Petäjä, T., Kerminen, V.-M., and Kulmala, M.: Sources and sinks driving sulphuric acid concentrations in contrasting environments: implications on proxy calculations, Atmos. Chem. Phys. Discuss., 10.5194/acp-2020-155, 2020a.

Dada, L., Lehtipalo, K., Kontkanen, J., Nieminen, T., Baalbaki, R., Ahonen, L., Duplissy, J., Yan, C., Chu, B., Petäjä, T., Lehtinen, K., Kerminen, V.-M., Kulmala, M., and Kangasluoma, J.: Formation and growth of sub-3-nm aerosol particles in experimental chambers, Nat Protoc, 15, 1013-1040, 10.1038/s41596-019-0274-z, 2020b.

Dai, L., Wang, H., Zhou, L., An, J., Tang, L., Lu, C., Yan, W., Liu, R., Kong, S., Chen, M., Lee, S., and Yu, H.: Regional and local new particle formation events observed in the Yangtze River Delta region, China, Journal of Geophysical Research: Atmospheres, 122, 2389-2402, 10.1002/2016jd026030, 2017.

Dal Maso, M., Kulmala, M., Riipinen, I., Wagner, R., Hussein, T., Aalto, P. P., and Lehtinen, K. E. J.: Formation and growth of fresh atmospheric aerosols: eight years of aerosol size distribution data from SMEAR II, Hyytiala, Finland, Boreal Environ Res, 10, 323-336, 2005.

Deng, C., Fu, Y., Dada, L., Yan, C., Cai, R., Yang, D., Zhou, Y., Yin, R., Lu, Y., Li, X., Qiao, X., Fan, X., Nie, W., Kontkanen, J., Kangasluoma, J., Chu, B., Ding, A., Kerminen, V. M., Paasonen, P., Worsnop, D. R., Bianchi, F., Liu, Y., Zheng, J., Wang, L., Kulmala, M., and Jiang, J.: Seasonal Characteristics of New Particle Formation and Growth in Urban Beijing, Environ Sci Technol, 54, 8547-8557, 10.1021/acs.est.0c00808, 2020a.

https://doi.org/10.5194/acp-2021-266
Preprint. Discussion started: 4 May 2021

Deng, C., Cai, R., Yan, C., Zheng, J., and Jiang, J.: Formation and growth of sub-3 nm particles in megacities: impact of background aerosols, Faraday Discuss, 10.1039/d0fd00083c, 2020b.

Ehn, M., Thornton, J.A., Kleist, E., Sipila, M., Junninen, H., Pullinen, I., Springer, M., Rubach, F., Tillmann, R., Lee, B., Lopez-Hilfiker, F., Andres, S., Acir, I.-H., Rissanen, M., Jokinen, T., Schobesberger, S., Kangasluoma, J., Kontkanen, J., Nieminen, T., Kurten, T., Nielsen, L. B., Jorgensen, S., Kjaergaard, H. G., Canagaratna, M., Maso, M. D., Berndt, T., Petaja, T., Wahner, A., Kerminen, V.-M., Kulmala, M., Worsnop, D. R., Wildt, J., and Mentel, T. F.: A large source of low-volatility secondary organic aerosol, Nature, 506, 476–479., 2014.

Du, W., Dada, L., Zhao, J., Chen, X., Daellenbach, K. R., Xie, C., Wang, W., He, Y., Cai, J., Yao, L., Zhang, Y., Wang, Q., Xu, W., Wang, Y., Tang, G., Cheng, X., Kokkonen, T. V., Zhou, W., Yan, C., Chu, B., Zha, Q., Hakala, S., Kurppa, M., Järvi, L., Liu, Y., Li, Z., Ge, M., Fu, P., Nie, W., Bianchi, F., Petäjä, T., Paasonen, P., Wang, Z., Worsnop, D. R., Kerminen, V.-M., Kulmala, M., and Sun, Y.: A 3D study on the amplification of regional haze and particle growth by local emissions, npj Climate and Atmospheric Science, 4, 4, 10.1038/s41612-020-00156-5, 2021.

Gao, Y., Zhang, D., Wang, J., Gao, H., and Yao, X.: Variations in Ncn and Nccn over China marginal seas related to marine traffic emissions, new particle formation and aerosol aging, Atmos. Chem. Phys., in press 2020.

Guo, S., Hu, M., Zamora, M. L., Peng, J. F., Shang, D. J., Zheng, J., Du, Z. F., Wu, Z., Shao, M., Zeng, L. M., Molina, M. J., and Zhang, R. Y.: Elucidating severe urban haze formation in China, P Natl Acad Sci USA, 111, 17373-17378, 10.1073/pnas.1419604111, 2014.

Guo, S., Hu, M., Peng, J., Wu, Z., Zamora, M. L., Shang, D., Du, Z., Zheng, J., Fang, X., Tang, R., Wu, Y., Zeng, L., Shuai, S., Zhang, W., Wang, Y., Ji, Y., Li, Y., Zhang, A. L., Wang, W., Zhang, F., Zhao, J., Gong, X., Wang, C., Molina, M. J., and Zhang, R.: Remarkable nucleation and growth of ultrafine particles from vehicular exhaust, Proc Natl Acad Sci U S A, 117, 3427-3432, 10.1073/pnas.1916366117, 2020.

Hamed, A., Korhonen, H., Sihto, S.-L., Joutsensaari, J., Järvinen, H., Petäjä, T., Arnold, F., Nieminen, T., Kulmala, M., Smith, J. N., Lehtinen, K. E. J., Laaksonen, A., and High relative humidity supresses contenental new particle formation events, 2010.

https://doi.org/10.5194/acp-2021-266
Preprint. Discussion started: 4 May 2021

Hamed, A., Korhonen, H., Sihto, S.-L., Joutsensaari, J., Järvinen, H., Petäjä, T., Arnold, F., Nieminen, T., Kulmala, M., Smith, J. N., Lehtinen, K. E. J., and Laaksonen, A.: The role of relative humidity in continental new particle formation, Journal of Geophysical Research, 116, 10.1029/2010jd014186, 2011.

Herrmann, E., Ding, A. J., Kerminen, V. M., Petäjä, T., Yang, X. Q., Sun, J. N., Qi, X. M., Manninen, H., Hakala, J., Nieminen, T., Aalto, P. P., Kulmala, M., and Fu, C. B.: Aerosols and nucleation in eastern China: first insights from the new SORPES-NJU station, Atmos Chem Phys, 14, 2169-2183, 10.5194/acp-14-2169-2014, 2014.

Hussein, T., Junninen, H., Tunved, P., Kristensson, A., Dal Maso, M., Riipinen, I., Aalto, P. P., Hansson, H. C., Swietlicki, E., and Kulmala, M.: Time span and spatial scale of regional new particle formation events over Finland and Southern Sweden, Atmos Chem Phys, 9, 4699-4716, 10.5194/acp-9-4699-2009, 2009.

Jun, Y.-S., Jeong, C.-H., Sabaliauskas, K., Richard Leaitch, W., and Evans, G. J.: A year-long comparison of particle formation events at paired urban and rural locations, Atmospheric Pollution Research, 5, 447-454, 10.5094/apr.2014.052, 2014.

Kangasluoma, J., Cai, R., Jiang, J., Deng, C., Stolzenburg, D., Ahonen, L. R., Chan, T., Fu, Y., Kim, C., Laurila, T. M., Zhou, Y., Dada, L., Sulo, J., Flagan, R. C., Kulmala, M., Petäjä, T., and Lehtipalo, K.: Overview of measurements and current instrumentation for 1–10 nm aerosol particle number size distributions, J Aerosol Sci, 148, 10.1016/j.jaerosci.2020.105584, 2020.

Kerminen, V. M., Chen, X. M., Vakkari, V., Petäjä, T., Kulmala, M., and Bianchi, F.: Atmospheric new particle formation and growth: review of field observations, Environ Res Lett, 13, https://doi.org/10.1088/1748-9326/aadf3c, 2018.

Komppula, M., Sihto, S.-L., Korhonen, H., Lihavainen, H., Kerminen, V.-M., Kulmala, M., and Viisanen, Y.: New particle formation in air mass transported between two measurement sites in Northern Finland, Atmos Chem Phys, 6, 14, www.atmos-chem-phys.net/6/2811/2006/, 2006.

Kontkanen, J., Deng, C., Fu, Y., Dada, L., Zhou, Y., Cai, J., Daellenbach, R.-K., Hakala, S., Kokkonen, V.-T., Lin, Z., Liu, Y., Wang, Y., Yan, C., Petäjä, T., Jiang, J., Kulmala, M and Paasonen, P.: Size-resolved particle number emissions in Beijing determined from measured particle size

https://doi.org/10.5194/acp-2021-266
Preprint. Discussion started: 4 May 2021

distributions, Atmospheric Chemistry and Physics, 20, 11329–11348, https://doi.org/10.5194/acp-20-11329-2020, 2020.

Kulmala, M., Vehkamaki, H., Petaja, T., Dal Maso, M., Lauri, A., Kerminen, V. M., Birmili, W., and McMurry, P. H.: Formation and growth rates of ultrafine atmospheric particles: a review of observations, J Aerosol Sci, 35, 143-176, 2004.

Kulmala, M., Petäjä, T., Nieminen, T., Sipilä, M., Manninen, H. E., Lehtipalo, K., Dal Maso, M., Aalto, P. P., Junninen, H., Paasonen, P., Riipinen, I., Lehtinen, K. E. J., Laaksonen, A., and Kerminen, V. M.: Measurement of the nucleation of atmospheric aerosol particles, Nat Protoc, 7, 1651-1667, https://doi.org/10.1038/nprot.2012.091, 2012.

Kulmala, M.: Atmospheric chemistry: China's choking cocktail, Nature, 526, 497-499, https://doi.org/10.1038/526497a, 2015.

Kulmala, M.: Build a global Earth observatory, Nature, 553, 21-23, https://doi.org/10.1038/d41586-017-08967-y, 2018.

Kulmala, M., Dada, L., Dällenbach, K., Yan, C., Stolzenburg, D., Kontkanen, J., Ezhova, E., Hakala, S., Tuovinen, S., Kokkonen, T., Kurppa, M., Cai, R., Zhou, Y., Yin, R., Baalbaki, R., Chan, T., Chu, B., Deng, C., Fu, Y., Ge, M., He, H., Heikkinen, L., Junninen, H., Nei, W., Rusanen, A., Vakkari, V., Wang, Y., Wang, L., yao, l., Zheng, J., Kujansuu, J., Kangasluoma, J., Petäjä, T., Paasonen, P., Järvi, L., Worsnop, D., Ding, A., Liu, Y., Jiang, J., Bianchi, F., Yang, G., Liu, Y., Lu, Y., and Kerminen, V.-M.: Is reducing new particle formation a plausible solution to mitigate particulate air pollution in Beijing and other Chinese megacities?, Faraday Discuss., 226, 334-347, 10.1039/d0fd00078g, 2021.

Lehtipalo, K., Leppä, J., Kontkanen, J., Kangasluoma, J., Wimmer, D., Franchin, A., Schobesberger, S., Junninen, H., Petäjä, T., Sipilä, M., Mikkilä, J., Vanhanen, J., Worsnop, D. r., and Kulmala, M.: methods for determining particle size distribution and growth rates between 1 and 3 nm using the Particle Size Magnifier, Boreal Environ Res, 19 215-236, 2014.

Lehtipalo, K., Yan, C., Dada, L., Bianchi, F., Xiao, M., Wagner, R., Stolzenburg, D., Ahonen, L. R., Amorim, A., Baccarini, A., Bauer, P. S., Baumgartner, B., Bergen, A., Bernhammer, A. K., Breitenlechner, M., Brilke, S., Buchholz, A., Mazon, S. B., Chen, D. X., Chen, X. M., Dias, A., Dommen, J., Draper, D. C., Duplissy, J., Ehn, M., Finkenzeller, H., Fischer, L., Frege, C., Fuchs, C.,

https://doi.org/10.5194/acp-2021-266
Preprint. Discussion started: 4 May 2021

Garmash, O., Gordon, H., Hakala, J., He, X. C., Heikkinen, L., Heinritzi, M., Helm, J. C., Hofbauer, V., Hoyle, C. R., Jokinen, T., Kangasluoma, J., Kerminen, V. M., Kim, C., Kirkby, J., Kontkanen, J., Kurten, A., Lawler, M. J., Mai, H. J., Mathot, S., Mauldin, R. L., Molteni, U., Nichman, L., Nie, W., Nieminen, T., Ojdanic, A., Onnela, A., Passananti, M., Petäjä, T., Piel, F., Pospisilova, V., Quéléver, L. L. J., Rissanen, M. P., Rose, C., Sarnela, N., Schallhart, S., Schuchmann, S., Sengupta, K., Simon, M., Sipilä, M., Tauber, C., Tomé, A., Tröstl, J., Väisänen, O., Vogel, A. L., Volkamer, R., Wagner, A. C., Wang, M. Y., Weitz, L., Wimmer, D., Ye, P. L., Ylisirnio, A., Zha, Q. Z., Carslaw, K. S., Curtius, J., Donahue, N. M., Flagan, R. C., Hansel, A., Riipinen, I., Virtanen, A., Winkler, P. M., Baltensperger, U., Kulmala, M., and Worsnop, D. R.: Multicomponent new particle formation from sulfuric acid, ammonia, and biogenic vapors, Sci Adv, 4, https://doi.org/10.1126/sciadv.aau5363, 2018.

Leino, K., Lampilahti, J., Poutanen, P., Väänänen, R., Manninen, A., Buenrostro Mazon, S., Dada, L., Franck, A., Wimmer, D., Aalto, P. P., Ahonen, L. R., Enroth, J., Kangasluoma, J., Keronen, P., Korhonen, F., Laakso, H., Matilainen, T., Siivola, E., Manninen, H. E., Lehtipalo, K., Kerminen, V.-M., Petäjä, T., and Kulmala, M.: Vertical profiles of sub-3 nm particles over the boreal forest, Atmos Chem Phys, 19, 4127-4138, 10.5194/acp-19-4127-2019, 2019.

Liu, J., Zhang, X. L., Xu, X. F., and Xu, H. H.: Comparison analysis of variation characteristics of SO2, NOx, O3 and PM2.5 between rural and urban areas, Beijing, Huan jing ke xue= Huanjing kexue / [bian ji, Zhongguo ke xue yuan huan jing ke xue wei yuan hui "Huan jing ke xue" bian ji wei yuan hui.], 29, 1059-1065, 2008.

Lu, Y., Yan, C., Fu, Y., Chen, Y., Liu, Y., Yang, G., Wang, Y., Bianchi, F., Chu, B., and Zhou, Y.: A proxy for atmospheric daytime gaseous sulfuric acid concentration in urban Beijing, Atmospheric Chemistry and Physics, 19, 1971-1983, 10.5194/acp-19-1971-2019, 2019.

Ma, L., Zhu, Y., Zheng, M., Sun, Y., Huang, L., Liu, X., Gao, Y., Shen, Y., Gao, H., and Yao, X.: Investigating three patterns of new particles growing to the size of cloud condensation nuclei in Beijing's urban atmosphere, Atmos Chem Phys, 21, 183-200, 10.5194/acp-21-183-2021, 2021.

Man, H., Zhu, Y., Ji, F., Yao, X., Lau, N. T., Li, Y., Lee, B. P., and Chan, C. K.: Comparison of Daytime and Nighttime New Particle Growth at the HKUST Supersite in Hong Kong, Environ Sci

https://doi.org/10.5194/acp-2021-266
Preprint. Discussion started: 4 May 2021

Atmospheric Chemistry and Physics Discussions
Open Access EGU

Technol, 49, 7170-7178, 10.1021/acs.est.5b02143, 2015.

Paasonen, P., Peltola, M., Kontkanen, J., Junninen, H., Kerminen, V.-M., and Kulmala, M.: Comprehensive analysis of particle growth rates from nucleation mode to cloud condensation nuclei in boreal forest, Atmos Chem Phys, 18, 12085-12103, 10.5194/acp-18-12085-2018, 2018.

Pierce, J. R., and Adams P. J.: Uncertainty in global CCN concentrations from uncertain aerosol nucleation and primary emission rates. Atmos. Chem. Phys., 9, 1339–1356, 10.5194/acp-9-1339-2009, 2009.

Qi, X., Ding, A., Roldin, P., Xu, Z., Zhou, P., Sarnela, N., Nie, W., Huang, X., Rusanen, A., Ehn, M., Rissanen, M. P., Petäjä, T., Kulmala, M., and Boy, M.: Modelling studies of HOMs and their contributions to new particle formation and growth: comparison of boreal forest in Finland and a polluted environment in China, Atmos Chem Phys, 18, 11779-11791, 10.5194/acp-18-11779-2018, 2018.

Qi, X. M. D., A. J., Nie, W., Petaja, T., Kerminen, V. M., Herrmann, E., Xie, Y. N., Zheng, L. F., Manninen, H., Aalto, P., Sun, J. N., Xu, Z. N., Chi, X. G., Huang, X., Boy, M., Virkkula, A., Yang, X. Q., Fu, C. B., and Kulmala, M.: Aerosol size distribution and new particle formation in the western Yangtze River Delta of China: 2 years of measurements at the SORPES station, Atmos Chem Phys, 15, 12445-12464, 2015.

Salma, I., Németh, Z., Kerminen, V.-M., Aalto, P., Nieminen, T., Weidinger, T., Molnár, Á., Imre, K., and Kulmala, M.: Regional effect on urban atmospheric nucleation, Atmos Chem Phys, 16, 8715-8728, 10.5194/acp-16-8715-2016, 2016.

Shen, X., Sun, J., Kivekäs, N., Kristensson, A., Zhang, X., Zhang, Y., Zhang, L., Fan, R., Qi, X., Ma, Q., and Zhou, H.: Spatial distribution and occurrence probability of regional new particle formation events in eastern China, Atmos Chem Phys, 18, 587-599, 10.5194/acp-18-587-2018, 2018.

Shen, X. J., Sun, J. Y., Zhang, Y. M., Wehner, B., Nowak, A., Tuch, T., Zhang, X. C., Wang, T. T., Zhou, H. G., Zhang, X. L., Dong, F., Birmili, W., and Wiedensohler, A.: First long-term study of particle number size distributions and new particle formation events of regional aerosol in the North China Plain, Atmos Chem Phys, 11, 1565-1580, 2011.

Stohl, A., Forster, C., Frank, A., Seibert, P., and Wotawa, G.: Technical note: The Lagrangian particle dispersion model FLEXPART version 6.2. , Atmospheric Chemistry and Physics 5, 24, 10.5194/acp-5-2461-2005., 2005.

Vana, M., Komsaare, K., Hõrrak, U., Mirme, S., Nieminen, T., Petäjä, T., Noe, S. M., Kontkanen, J., Manninen, H. E., and Kulmala, M.: Characteristics of new-particle formation at three SMEAR stations, Boreal Environ Res, 21, 17, 2016.

Wang, J., Shen, Y., Li, K., Gao, Y., Gao, H., and Yao, X.: Nucleation-mode particle pool and large increases in Ncn and Nccn observed over the northwestern Pacific Ocean in the spring of 2014. , Atmos. Chem. Phys., 19, 17, https://doi.org/10.5194/acp-19-8845-2019, 2019.

Wang, M., Zhu, T., Zhang, J. P., Zhang, Q. H., Lin, W. W., Li, Y., and Wang, Z. F.: Using a mobile laboratory to characterize the distribution and transport of sulfur dioxide in and around Beijing, Atmos Chem Phys, 11, 11631-11645, 2011.

Wang, Z. B., Hu, M., Sun, J. Y., Wu, Z. J., Yue, D. L., Shen, X. J., Zhang, Y. M., Pei, X. Y., Cheng, Y. F., and Wiedensohler, A.: Characteristics of regional new particle formation in urban and regional background environments in the North China Plain, Atmos Chem Phys, 13, 12495-12506, 10.5194/acp-13-12495-2013, 2013.

Wang, Z. B., Wu, Z. J., Yue, D. L., Shang, D. J., Guo, S., Sun, J. Y., Ding, A. J., Wang, L., Jiang, J. K., Guo, H., Gao, J., Cheung, H. C., Morawska, L., Keywood, M., and Hu, M.: New particle formation in China: Current knowledge and further directions, Science of the Total Environment, 577, 258-266, 2017.

Wu, Z., Hu, M., Liu, S., Wehner, B., Bauer, S., Ma ßling, A., Wiedensohler, A., Petäjä, T., Dal Maso, M., and Kulmala, M.: New particle formation in Beijing, China: Statistical analysis of a 1-year data set, Journal of Geophysical Research, 112, 10.1029/2006jd007406, 2007.

Yang-Chun, Y., Bo, H., and Wang, Y.: Changing Characteristics of the Main Air Pollutants of the Dongling Mountain in Beijing, Environmental Science, 34, 8, 2013.

Yao, L., Garmash, O., Bianchi, F., Zheng, J., Yan, C., Kontkanen, J., Junninen, H., Mazon, S. B., Ehn, M., Paasonen, P., Sipilä, M., Wang, M. Y., Wang, X. K., Xiao, S., Chen, H. F., Lu, Y. Q., Zhang, B. W., Wang, D. F., Fu, Q. Y., Geng, F. H., Li, L., Wang, H. L., Qiao, L. P., Yang, X., Chen, J. M., Kerminen, V. M., Petäjä, T., Worsnop, D. R., Kulmala, M., and Wang, L.: Atmospheric new particle

Atmospheric Chemistry and Physics Discussions

formation from sulfuric acid and amines in a Chinese megacity, Science, 361, 278-281, https://doi.org/10.1126/science.aao4839, 2018.

Yao, L., Fan, X., Yan, C., Kurtén, T., Daellenbach, K. R., Li, C., Wang, Y., Guo, Y., Dada, L., Rissanen, M. P., Cai, J., Tham, Y. J., Zha, Q., Zhang, S., Du, W., Yu, M., Zheng, F., Zhou, Y., Kontkanen, J., Chan, T., Shen, J., Kujansuu, J. T., Kangasluoma, J., Jiang, J., Wang, L., Worsnop, D. R., Petäjä, T., Kerminen, V.-M., Liu, Y., Chu, B., He, H., Kulmala, M., and Bianchi, F.: Unprecedented Ambient Sulfur Trioxide (SO3) Detection: Possible Formation Mechanism and Atmospheric Implications, Environ Sci Tech Let, 7, 809-818, 10.1021/acs.estlett.0c00615, 2020.

Ying, G., Ma, J., and Xing, Y.: Comparison of air quality management strategies of PM10, SO2, and NOx by an industrial source complex model in Beijing, Environmental Progress, 26, 33-42, 2010.

Yu, F. and Luo, G.: Simulation of particle size distribution with a global aerosol model: contribution of nucleation to aerosol and CCN number concentrations, Atmos. Chem. Phys., 9, 7691–7710, 10.5194/acp-9-7691-2009, 2009.

Zhang, R., Khalizov, A., Wang, L., Hu, M., and Xu, W.: Nucleation and growth of nanoparticles in the atmosphere, Chemical Reviews, 112, 1957-2011, 10.1021/cr2001756, 2012.

Zhou, Y., Dada, L., Liu, Y., Fu, Y., Kangasluoma, J., Chan, T., Yan, C., Chu, B., Daellenbach, K. R., Bianchi, F., Kokkonen, T. V., Liu, Y., Kujansuu, J., Kerminen, V.-M., Petäjä, T., Wang, L., Jiang, J., and Kulmala, M.: Variation of size-segregated particle number concentrations in wintertime Beijing, Atmos Chem Phys, 20, 1201-1216, 10.5194/acp-20-1201-2020, 2020.

Zimmerman, N., Jeong, C.-H., Wang, J. M., Ramos, M., Wallace, J. S., and Evans, G. J.: A source-independent empirical correction procedure for the fast mobility and engine exhaust particle sizers, Atmos. Environ., 100, 7, 838 10.1016/j.atmosenv.2014.10.054, 2015., 2015.

https://doi.org/10.5194/acp-2021-266
Preprint. Discussion started: 4 May 2021

Atmospheric Chemistry and Physics Discussions
Open Access
EGU

7 Tables and Figures

Table 1: NPF event and non- event days during our observation at both stations.

Date	Type	Air masses (9:00-15:00)		$GR_{7\text{-}15nm}$ (nm/h)		J_7 ($cm^{-3}s^{-1}$)		Event Start (LT)		Ending diameter (nm)	
		UB	**MT**	**UB**	**MT**	**UB**	**MT**	**UB**	**MT**	**UB**	**MT**
2019/06/14	a	North	North	8.61	-	4.97	-	9:00	8:00	71	-
2019/06/15*	a	Local	Local	12.63	-	5.56	-	11:00	15:00	82	60
2019/06/17	d	East	Local								
2019/06/18	c	Local	West		10.5		0.17		12:00		45
2019/06/19	d	South	Local								
2019/06/21	d	East	Local								
2019/06/23	e	East	East								
2019/06/24	f	Local	Local		8.21		-		12:00		50
2019/06/25*	a	Local	Local	-	-	-	-	12:00	15:00	-	53
2019/06/28	g	West	West	-		-		11:00			
2019/06/29	a	North	North	12.93	7.14	6.93	2.28	9:00	8:00	21	19
2019/06/30	a	North	North	4.82	6.57	9.86	1.37	6:30	9:30	31	25
2019/07/01	a	North	North	7.31	5.82	3.84	0.82	9:00	8:30	105	102
2019/07/02	d	Local	West								
2019/07/03	a	North	North	7.89	6.52	3.25	0.75	9:00	8:00	72	46
2019/07/04	b	Local	Local	-		-		10:00			53
2019/07/06	a	North	North	7.39	6.51	9.21	1.75	7:00	9:30	25	19
2019/07/07	b	North	North	7.61		3.61		9:00		32	
2019/07/08	d	East	East								
2019/07/09	d	East	East								
2019/07/10	h	East	East								
2019/07/11	d	East	East								
2019/07/12	f	East	East		5.57		0.37		9:30		24
2019/07/13	c	Local	North		6.32		0.70		10:00		30
2019/07/14	a	North	North	12.04	9.86	3.91	0.89	11:30	9:30	63	47

'a' means NPF event observed at both stations, 'b' means NPF event day at UB station while non-event day at MT station, 'c' means NPF event day at MT station while non-event day at UB station, 'd' means non-event day at both stations on the same day, 'e' means undefined day at both stations, 'f' means undefined day at UB station while NPF event day at MT station, g means undefined day at MT station while NPF event day at UB station, h means undefined day at UB station while non-event day at MT station, * means NPF event observed at MT station was transported from somewhere else. – means the values cannot be reliably calculated. Only days when particle number size distribution were valid are included in this table.

https://doi.org/10.5194/acp-2021-266
Preprint. Discussion started: 4 May 2021

Atmospheric Chemistry and Physics Discussions
Open Access
EGU

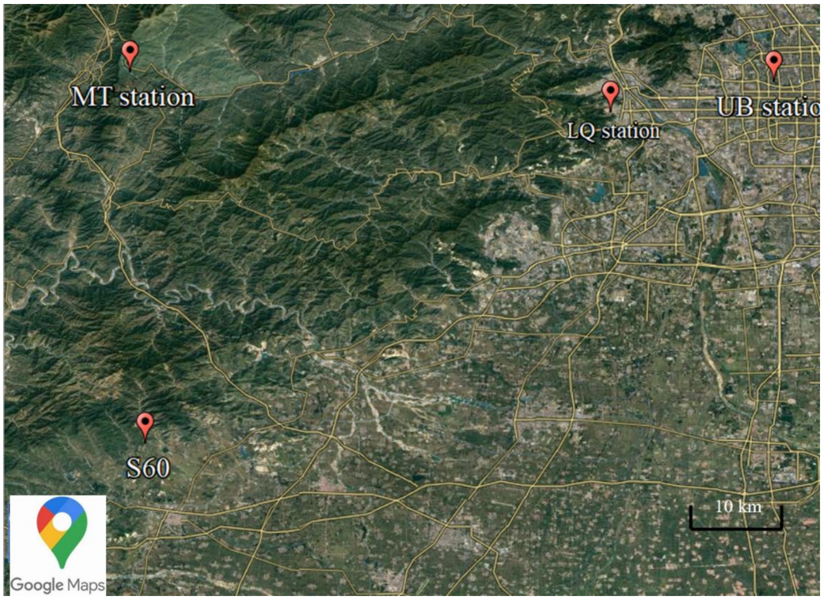

Figure 1: Map showing locations of urban station (UB), Longquan station (LQ), mountain station (MT) and another site 60 km south from MT station (S60). Figure produced using © Google Maps (https://maps.google.com).

https://doi.org/10.5194/acp-2021-266
Preprint. Discussion started: 4 May 2021

Atmospheric Chemistry and Physics
Discussions

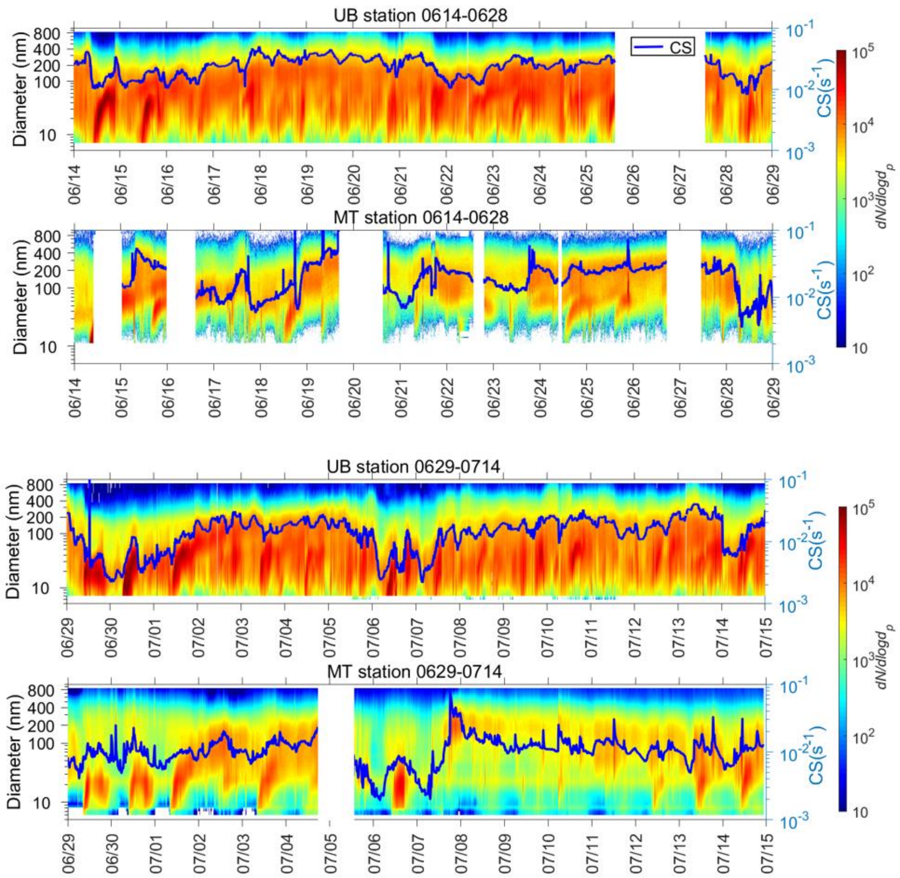

Figure 2: Time series of particle number size distribution and CS (the blue line) at UB and MT stations during our observations. Time resolutions for particle number size distribution data and CS were 8 min at UB station and 4 min at MT station, respectively.

https://doi.org/10.5194/acp-2021-266
Preprint. Discussion started: 4 May 2021

Atmospheric Chemistry and Physics Discussions

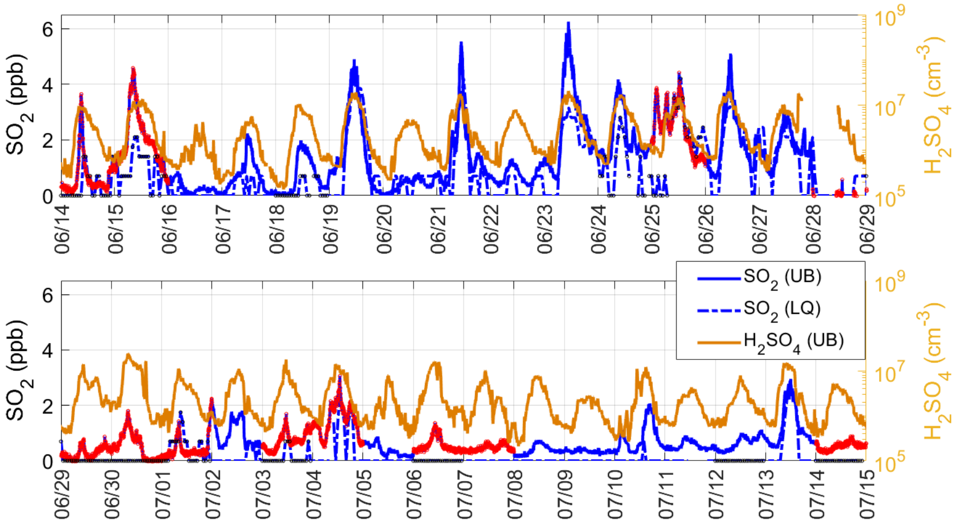

Figure 3: Time series of SO_2 concentration (ppb) at UB station and Longquan station (LQ) during our observation (left axis) as well as H_2SO_4 concentration measured at UB station (right axis). Data under detection limit are set as zero at both stations. Data on NPF event days were marked in red at UB station and black at MT station. Time resolution for SO_2 data was 5 min at UB station and 1h at LQ station, respectively.

https://doi.org/10.5194/acp-2021-266
Preprint. Discussion started: 4 May 2021

Atmospheric Chemistry and Physics
Open Access
Discussions

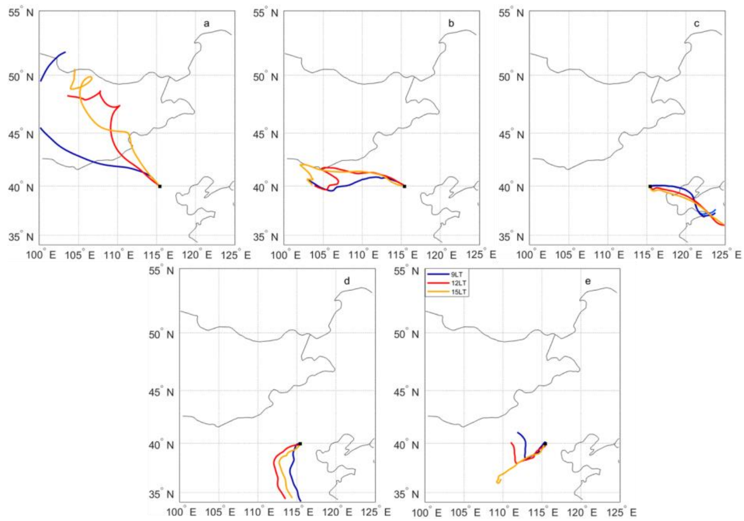

Figure 4: Examples of air masses arrived at both stations from (a) North group, (b) West group, (c) East group, (d) South group and (d) Local group during 9:00-15:00 (local time, LT). Both stations are under the same marker.

https://doi.org/10.5194/acp-2021-266
Preprint. Discussion started: 4 May 2021

Atmospheric Chemistry and Physics
Discussions
Open Access
EGU

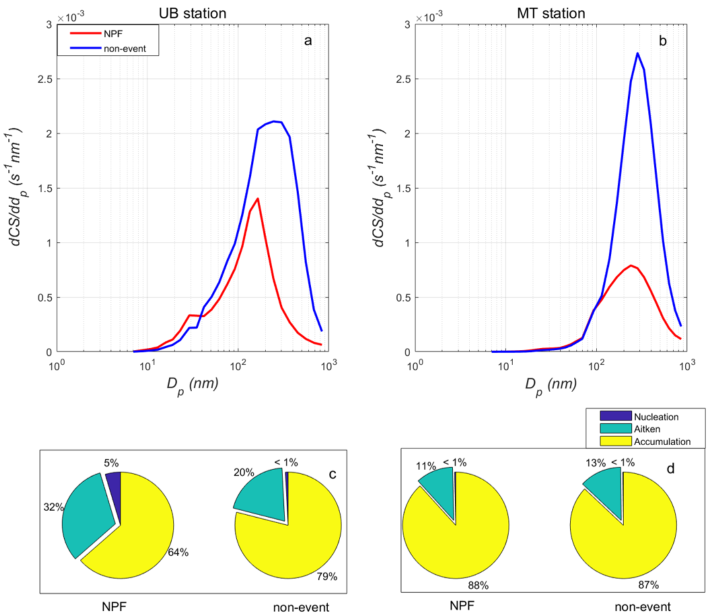

Figure 5: Median CS size distribution at UB (a) and MT (b) stations on NPF event and non-event days, respectively during 9:00-15:00 (local time, LT) and median contribution of nucleation, Aitken and accumulation mode particles to total CS at UB (c) and MT (d) stations on NPF event and non-event days, respectively during 9:00-15:00 (local time, LT). The time resolutions for CS and particle number concentration data were 8 min at UB station and 4 min at MT station, respectively.

https://doi.org/10.5194/acp-2021-266
Preprint. Discussion started: 4 May 2021

Atmospheric Chemistry and Physics Discussions

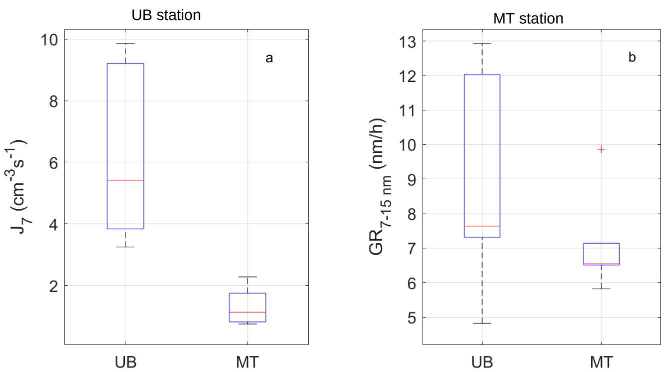

Figure 6: Median and percentiles of particle formation rates of 7 nm (J_7, $cm^{-3}s^{-1}$) and growth rates (GR, nm/h) of 7-15 nm for common NPF events. The time resolution for particle formation rates was 8 min at UB station and 4 min at MT station, respectively. We only took J_7 during the first 2 hours of every NPF event at each station on every NPF event day. The red line represents the median of the data and the lower and upper edges of the box represent 25th and 75th percentiles of the data, respectively. The length of the whiskers represents 1.5× interquartile range which includes 99.3% of the data.

https://doi.org/10.5194/acp-2021-266
Preprint. Discussion started: 4 May 2021

Atmospheric Chemistry and Physics
Discussions

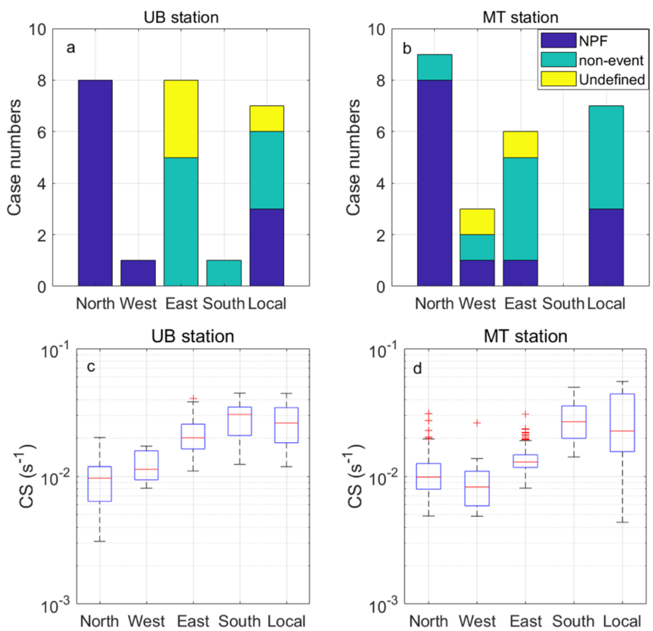

Figure 7: Occurrence of NPF events and non-events under air masses arriving from different directions at (a) UB and (b) MT stations. Medians and percentiles of condensation sink (CS, s^{-1}) under different air masses at (c) UB and (d) MT stations during the first 2h of NPF time window (9:00-11:00, local time). The red line represents the median of the data and the lower and upper edges of the box represent 25th and 75th percentiles of the data, respectively. The length of the whiskers represents 1.5× interquartile range which includes 99.3% of the data. Data outside the whiskers are considered outliers and are marked with red crosses. The time resolution of CS was 8 min at UB station and 4 min at MT station, respectively.

https://doi.org/10.5194/acp-2021-266
Preprint. Discussion started: 4 May 2021

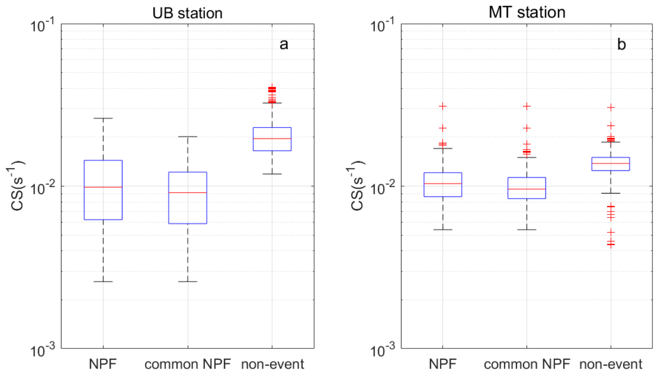

Figure 8: Medians and percentiles of condensation sink (CS, s^{-1}) at (a) UB and (b) MT stations during the first 2 hours of every NPF event and 9:00-11:00 (local time) on non-event days. The time resolution of CS was 8 min at UB station and 4 min at MT station, respectively. The red line represents the median of the data and the lower and upper edges of the box represent 25th and 75th percentiles of the data, respectively. The length of the whiskers represents 1.5 × interquartile range which includes 99.3% of the data. Data outside the whiskers are considered outliers and are marked with red crosses.

https://doi.org/10.5194/acp-2021-266
Preprint. Discussion started: 4 May 2021

Atmospheric Chemistry and Physics Discussions

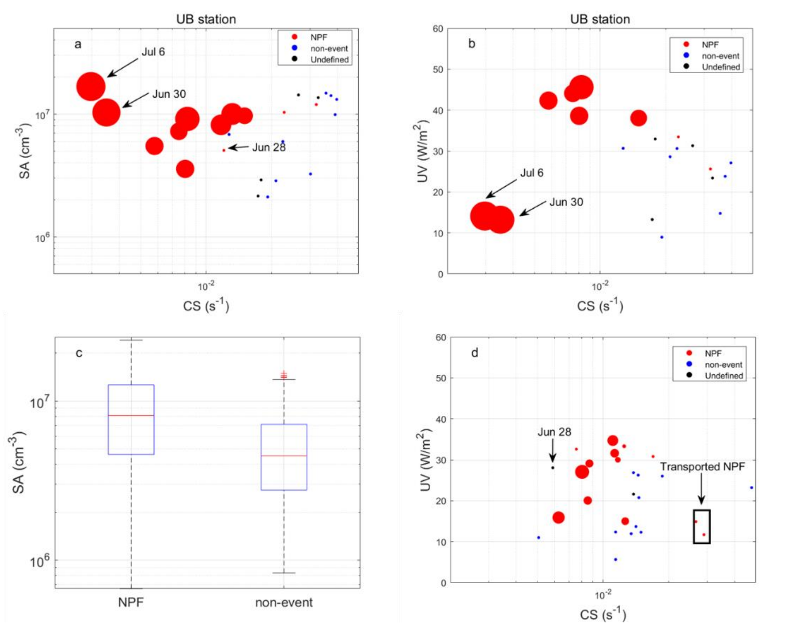

Figure 9: (a) Median condensation sinks (CS, s^{-1}) and H_2SO_4 concentration (SA, cm^{-3}) and (b) solar radiation (UVA+UVB, W/m^2) during the first 2 hours of every NPF event and 9:00-11:00 on every non-event day at UB station. (c) medians and percentiles of H_2SO_4 concentration observed at UB station during the first 2 hours of NPF events and 9:00-11:00 on non-event days. (d) Median condensation sinks (CS, s^{-1}) and solar radiation (UVA+UVB, W/m^2) during the first 2 hours of every NPF event and 9:00-11:00 on every non-event day at MT station. Transported NPF event cases and one non-event day with air masses belonging to west group (Jun 28) were all pointed out in the figure. Size of data points on NPF event days means particle formation rate (J_7, $cm^{-3}s^{-1}$) when it can be calculated reliably. The time resolution of CS was 8 min at UB station and 4 min at MT station, respectively. The time resolution was 30 min for SA data at UB station and 1h for solar radiation data at both stations.

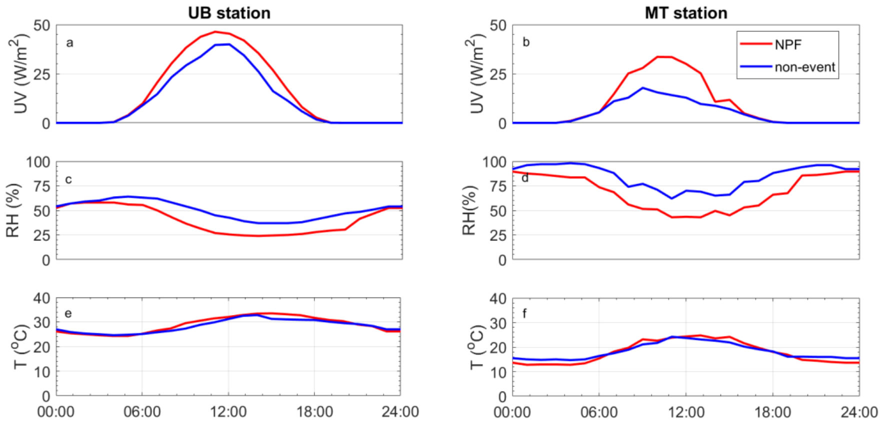

Figure 10: (a, b) Diurnal pattern of solar radiation (UV, W/m^2), (c, d) Temperature (T, °C), and (e, f) Relative humidity (RH, %), at UB (left panel) and MT (right panel) stations on both NPF event and non-event days. Time resolutions for all data points here were 1h.

https://doi.org/10.5194/acp-2021-266
Preprint. Discussion started: 4 May 2021

Atmospheric Chemistry and Physics
Open Access
EGU
Discussions

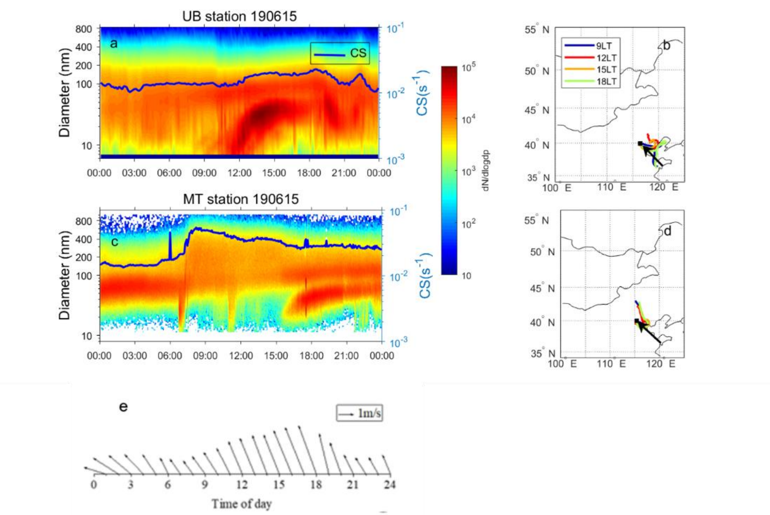

Figure 11: Time series of particle number size distribution, CS (blue lines) and air masses arrived at UB (upper panel) and MT (bottom panel) stations as well as wind conditions at MT station on June 15, 2019. Time resolution for particle number size distribution data and CS were both 8 min at UB station and 4 min at MT station, respectively. Time resolution for wind condition data was 1h at MT station. The arrows in the figure denotes directions of prevailing air masses before arriving at both stations during 9:00-15:00 LT.

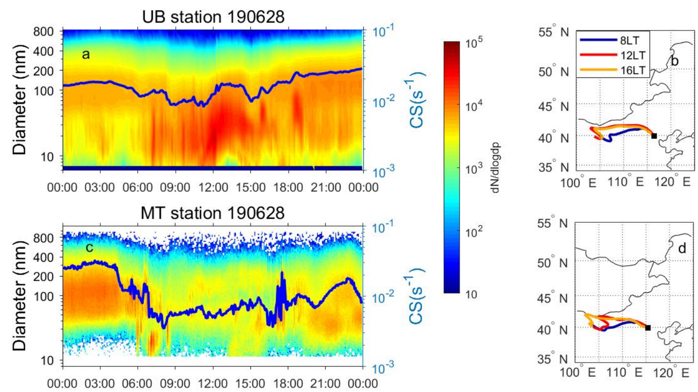

Figure 12: Time series of particle number size distribution, CS and air masses arrived at UB (upper panel) and MT (bottom panel) stations on June 28, 2019. Time resolution for particle number size distribution data and CS were both 8 min at UB station and 4 min at MT station, respectively.